Electron backscatter diffraction on femtosecond laser sulfur hyperdoped silicon

Thomas Gimpel, Ingmar Höger, Fritz Falk, Wolfgang Schade, and Stefan Kontermann

Citation: Applied Physics Letters **101**, 111911 (2012); doi: 10.1063/1.4752454
View online: http://dx.doi.org/10.1063/1.4752454
View Table of Contents: http://scitation.aip.org/content/aip/journal/apl/101/11?ver=pdfcov
Published by the AIP Publishing

Electron backscatter diffraction on femtosecond laser sulfur hyperdoped silicon

Thomas Gimpel,[1,a),b)] Ingmar Höger,[2] Fritz Falk,[2] Wolfgang Schade,[1] and Stefan Kontermann[1]
[1]*Fraunhofer Heinrich Hertz Institute (HHI), Am Stollen 19B, D-38640 Goslar, Germany*
[2]*Institute of Photonic Technology, Albert Einstein Straße 9, D-07745 Jena, Germany*

(Received 30 May 2012; accepted 30 August 2012; published online 14 September 2012)

This paper analyzes the impact of femtosecond laser pulse irradiation on the crystallinity of silicon wafers by means of electron backscatter diffraction (EBSD) measurements. EBSD based image quality maps and orientation imaging microscopy maps are correlated to the grade of the silicon crystallinity. We analyze the impact of accumulated net laser irradiation originating from a laser spot overlap that is necessary to process macroscopic areas, e.g., for sulfur doping of semiconductor devices. Furthermore, we demonstrate that post processing annealing recovers crystallinity and therefore allows fs-laser processed silicon to be used in semiconductor device manufacturing. © *2012 American Institute of Physics*. [http://dx.doi.org/10.1063/1.4752454]

Technical progress is increasingly relying on functionalized semiconductor surfaces in nearly all fields of applied science.[1] Nanostructuring silicon with femtosecond (fs)-laser pulses is a method for changing material characteristics like morphology,[2,3] hydrophobicity,[4] absorption,[5,6] and doping.[7,8] These characteristics find applications in advanced photovoltaic structures,[9] intermediate band photovoltaics,[5,10] and near infrared silicon photodiodes.[11,12] However, during fs-laser processing, the crystallinity of the substrate is deteriorated.[13,14] The reasons are extreme non-equilibrium processes induced by the intense light-matter interactions, resulting in a surface layer of amorphous, polymorphic, and nanocrystalline phases.[6,15] This is in contrast to laser treatment with nanosecond laser pulses which leads to classical melting of a surface layer followed by epitaxial recrystallization.[13] The loss of crystallinity originating from the fs-laser treatment decreases the charge carrier life time[16] in the substrate and hence the performance of manufactured semiconductor devices. However, under a sulfuric atmosphere,[11,12] only pulses in the fs regime are known to incorporate electrically active sulfur for doping purposes. The mechanism of amorphization of crystalline silicon depends first on the pulse duration.[17] The second significant parameter is the number of pulses hitting the surface. Lowest crystal deterioration is obtained for single laser pulse processing in which only one laser pulse is applied per laser spot.[18,19] For obtaining macroscopic areas with a homogenous laser induced surface structure and lateral homogenous sulfur doping, it is necessary that laser spots within a line and adjacent lines overlap. This work investigates the influence of the required overlap between subsequent laser pulses on the resulting amorphization, and methods to obtain optimum crystallinity on large areas. Electron backscatter diffraction (EBSD) is used[20,21] for mapping the crystallinity on large areas. Previous transmission electron microscopy (TEM) investigations[11,22,23] offer a very high resolution but are often limited to rather small regions.

For processing monocrystalline silicon Si-(100) substrates, a commercially available Mantis seed laser from Coherent and a Spitfire regenerative amplifier from Spectra Physics with a repetition rate of 10 kHz at a wavelength of 800 nm are used at fluencies of $E \approx 1.6\,\mathrm{J/cm^2}$. The sample is processed in a sulfur hexafluoride (SF_6) ambient at a pressure of $p = 0.66$ bar. EBSD analysis is performed in a Tescan Lyra XMU dual beam microscope equipped with an EDAX/TSL XM4 camera. Data are acquired and processed with the software package TSL OIM 5. The electron acceleration voltage is 30 kV, which corresponds to a maximum probing depth of $d_{\max} = 50$ nm. Information on crystallinity therefore is gathered from a surface near layer of this depth. The resolution is optimized to cover a macroscopic area of approximately $200 \times 100\,\mu\mathrm{m}^2$. We choose a pixel step pitch of $D = 2\,\mu$m at an electron beam spot size of $D_{Spot} \approx 310$ nm. In addition, higher resolution spot checks are performed all over the sample area with a pixel step pitch of $D = 0.1\,\mu$m at a spot size of $D_{Spot} \approx 95$ nm to validate that the coarse resolution does not lead to misinterpretations. Therefore, all amorphous appearing areas could as well consist of grains smaller than $0.1\,\mu$m. An amorphous layer thicker than the probing depth $d_{\max} = 50$ nm will lead to randomly colored pixels in the orientation imaging microscopy (OIM)[20] map. EBSD image quality (IQ) maps allow an even more sensitive contrast between the amorphous and the crystalline phase.[21] The correlation between IQ value and grade of crystallinity is depicted in Fig. 1, where we map amorphous thin film layers deposited by plasma enhanced chemical vapor deposition (PECVD) on top of a monocrystalline silicon substrate. An increasing thickness of the amorphous film results in a decreasing IQ value and a darker coloring within the map. A black gray scale value occurs, when the thickness of the amorphous film exceeds the probing depth of $d_{\max} = 50$ nm.

For sample processing, the laser spot is scanned with different overlaps across the sample with one pulse per spot. The top row of Figure 2(a) shows a scanning electron

[a)]Author to whom correspondence should be addressed. Electronic mail: thomas.gimpel@hhi.fraunhofer.de. Telephone: +49 53216855118.
[b)]This research was performed while Thomas Gimpel was at Energie-Forschungszentrum Niedersachsen, Am Stollen 19B, D-38640 Goslar, Germany.

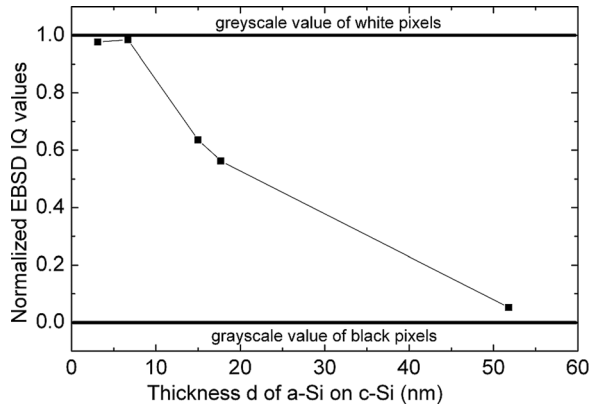

FIG. 1. Normalized EBSD IQ value versus the thickness of an amorphous layer on top of a monocrystalline silicon substrate. The value 1 corresponds to white pixels within the IQ maps, meaning the measured spot to be crystalline; 0 values are black pixels within the IQ maps, meaning the measured spot to consist of an amorphous layer thicker than the probing depth $d_{max} = 50\,nm$.

microscopy (SEM) image of single fs-laser pulses applied subsequently in a line with a step pitch of $L = 150\,\mu m$. The laser spot diameter is measured (intensity 1/e) to be $60\,\mu m$ but the surface is modified in a diameter of approximately $160\,\mu m$, which is already below the 5 %-intensity level. For the fluency of $E \approx 1.6\,J/cm^2$, the 1/e-intensity level (corresponding to a fluence of $E \approx 0.6\,J/cm^2$) is near the known threshold for ablation and recrystallization[18] and the 5 %-intensity level (corresponding to a fluence of $E \approx 0.08\,J/cm^2$) is near the threshold for single shot surface modification or rather amorphization.[23] Within the SEM picture of Fig. 2(a), these thresholds appear as two rings, although the spot shape reveals not to be completely concentric circular. Another striking contrast appears within the area of the overlap. Exactly, these areas form the main contrast within the EBSD IQ map in the bottom row of Fig. 2(a), which indicates this area to be amorphous. The dashed rings in Fig. 2(a) highlight an area that features a very slight difference in contrast compared to the surrounding area. The position of these rings corresponds to the above mentioned intensity levels appearing as relief in the SEM image with diameters of $60\,\mu m$ and $160\,\mu m$. This low contrast shows that these two rings consist of amorphous material less than 10 nm thick. The higher contrast within the area of the overlap shows that the amorphous layer is thicker than 10 nm there. Any other area within the thin amorphous rings is found to be homogenously white meaning the material is crystalline. Recrystallization takes place in these areas. This reveals that amorphization by a subsequent laser pulse in the area of the overlap plays a more important role than the amorphization by a single pulse. The grade of amorphization increases with the overlap. In the bottom row of Fig. 2(b), a row of single fs-laser pulses with a step pitch of $L = 80\,\mu m$ is mapped via EBSD IQ and OIM. This step pitch is of interest because then the spots, where ablation and recrystallization recovers the substrate's crystallinity, are very close to each other and remaining amorphization is at a minimum. Moreover, it is close enough to modify the surface almost homogenously, in particular for area scanned samples. The inset within the EBSD IQ map of Fig. 2(b) shows the homogenously red colored OIM map indicating that no amorphous layer occurs that exceeds the probing depth. However, the IQ map shows dark areas indicating thin amorphous layers within the probing depth. But for this overlapped spots, the depicted structures feature amorphous material thicker than 10 nm, as it appears darker than the low contrast rings in the IQ map of Fig. 2(a). To better understand the "Double-C"-shape of these darker structures, the dashed circles in Fig. 2(b) mark the two rings of the original spot as in Fig. 2(a). The smaller "C"-shape, which is almost a full circle, has a diameter of $60\,\mu m$ and corresponds to the ablation and recrystallization spot as the inner ring in Fig. 2(a). The elongated "C"-shape structure has a lengthwise dimension of about $160\,\mu m$ and therefore obviously develops from the outer ring of the original single spot. It is not a full circle because the overlap of

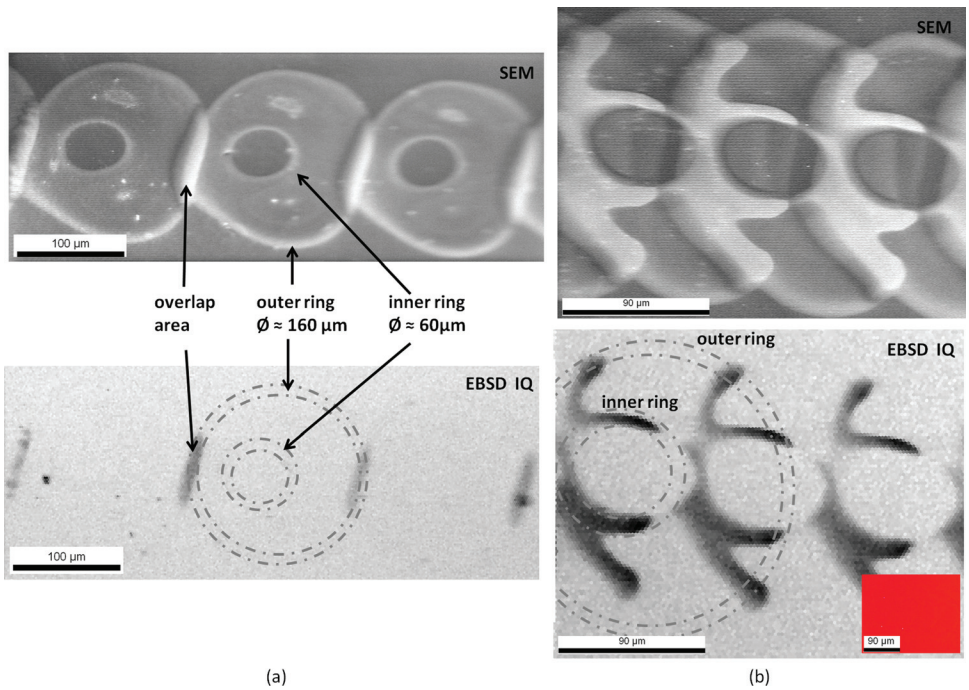

FIG. 2. Single fs-laser pulse lines with a step pitch of (a) $L = 150\,\mu m$ and (b) $L = 80\,\mu m$. Top row: SEM images; bottom row: EBSD IQ maps. Dashed rings mark interface boundary area of the ablation and recrystallization threshold (inner ring) and the modification threshold (outer ring) which both form a low contrast within the EBSD IQ map, meaning this areas to be amorphous with a thickness less than 10 nm (inset in the IQ map of (b): OIM map indicating red areas to be (100) oriented and amorphous material to be thinner than the probing depth).

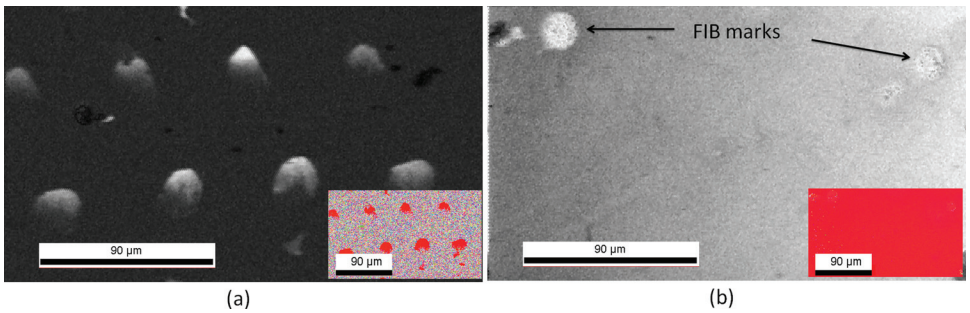

FIG. 3. EBSD maps of a monocrystalline silicon sample after an area scan with fs-laser pulses (same overlap as in Fig. 2(b)). (a) IQ map of the non-annealed sample. (b) IQ map of the same sample after annealing at $T = 800\,^{\circ}\mathrm{C}$ for $t = 30$ min. Insets: OIM maps indicating red areas to be (100) oriented.

the subsequent laser pulse does not cover the whole ring and amorphization is therefore not intensified all over. The overlap area is hit by two subsequent laser pulses and multi shot amorphization[17,23] intensifies the low amorphization that is already present after a single pulse. That means overlapping shots lead to an extra amorphization. When we proceed from the single pulse line of Fig. 2(b) to large area processing, adjacent lines create an additional overlap compared to the overlap originating from spots within a single line, resulting again in an extra amorphization. This additional extra amorphization leads to the EBSD IQ map shown in Fig. 3(a), where a large fraction of the area is amorphous, displayed in black. The amorphous layer obviously reaches depths larger than the probing depth so that even the OIM map switches its color as can be seen in the inset of Fig. 3(a). Nevertheless, monocrystalline spots remain. These spots are located in the centers of the laser spots, where the recrystallisation threshold is exceeded. The fluence of subsequent laser spots, which hit these monocrystalline spots due to the overlap, is either below the modification threshold or within the recrystallized areas. The amorphous material, which is present in the fs-laser pulse line, is now further intensified by a third and even a fourth irradiation event due to the overlap. These are reasons why the monocrystalline fraction is clearly smaller on an area-scanned sample as compared to the single fs-laser pulse line of Fig 2(b). A substantial improvement of the crystal quality requires optimization of the overlap, or, even better, a beam with top hat profile, where no overlap is necessary. Concerning optoelectronic device fabrication, annealing processes are common. It is well known that amorphous silicon crystallizes at temperatures above $T \approx 600\,^{\circ}\mathrm{C}$.[24,25] Figure 3(b) shows the same area as imaged in Fig. 3(a) after annealing at $T = 800\,^{\circ}\mathrm{C}$ for $t = 30$ min. For identification purpose, focused ion beam (FIB) marks are set as shown in Fig. 3(b). The EBSD OIM map shows the substrate orientation all over the area. This implies a heavy reduction of the amorphous layer thickness. Even the EBSD IQ map of Fig. 3(b) is homogenously lit up, except at the FIB-marks in the corners of the image. The same effect of annealing occurs for the line scans of Figs. 2(a) and 2(b) (not shown here). Obviously, during annealing epitaxial crystal growth occurred from the substrate, which serves as a seed.[25]

In conclusion, when silicon is processed with single fs-laser pulses, amorphization occurs at the tails of the laser spots. For large area processing, overlapping laser spots are applied subsequently. In the overlap regions, several irradiation events with low fluence lead to a heavy extra amorphization. Nevertheless, monocrystalline areas always exist for the used process parameters at the centers of the individual laser spots. By post processing annealing, the complete area can be recrystallized to the substrate orientation. Our results show how to improve the crystal quality of fs-laser structured functionalized semiconductor material.

[1]F. Tao and S. Bernasek, *Functionalization of Semiconductor Surfaces* (John Wiley & Sons, Hoboken, NJ, 2012).
[2]T.-H. Her, R. J. Finlay, C. Wu, S. Deliwala, and E. Mazur, Appl. Phys. Lett. **73**, 1673 (1998).
[3]M. Y. Shen, C. H. Crouch, J. E. Carey, R. Younkin, E. Mazur, M. A. Sheehy, and C. M. Friend, Appl. Phys. Lett. **82**, 1715 (2003).
[4]T. Baldacchini, J. E. Carey, M. Zhou, and E. Mazur, Langmuir **22**, 4917 (2006).
[5]M. A. Sheehy, B. R. Tull, C. M. Friend, and E. Mazur, Mater. Sci. Eng., B **137**, 289 (2007).
[6]C. H. Crouch, J. E. Carey, M. Shen, E. Mazur, and F. Y. Génin, Appl. Phys. A **79**, 1635 (2004).
[7]M.-J. Sher, M. T. Winkler, and E. Mazur, MRS Bull. **36**, 439 (2011).
[8]J. E. Carey, C. H. Crouch, and E. Mazur, Opt. Photonics News **14**, 32 (2003).
[9]J. Zhao, A. Wang, M. A. Green, and F. Ferrazza, Appl. Phys. Lett. **73**, 1991 (1998).
[10]B. K. Newman, J. Sullivan, M. T. Winkler, M. Sher, M. A. Marcus, S. Fakra, M. J. Smith, S. Gradečak, E. Mazur, and T. Buonassisi, in *Proceedings of the 24th European Photovoltaic Solar Energy Conference (EUPVSEC)*, Hamburg, Germany (2009), pp. 236–238.
[11]J. E. Carey, C. H. Crouch, M. Y. Shen, and E. Mazur, Opt. Lett. **30**, 1773 (2005).
[12]Z. Huang, J. E. Carey, M. Liu, X. Guo, E. Mazur, and J. C. Campbell, Appl. Phys. Lett. **89**, 33506 (2006).
[13]C. H. Crouch, J. E. Carey, J. M. Warrender, M. J. Aziz, E. Mazur, and F. Y. Génin, Appl. Phys. Lett. **84**, 1850 (2004).
[14]J. Jia, M. Li, and C. V. Thompson, Appl. Phys. Lett. **84**, 3205 (2004).
[15]M. J. Smith, Y.-T. Lin, M.-J. Sher, M. T. Winkler, E. Mazur, and S. Gradečak, J. Appl. Phys **110**, 53524 (2011).
[16]R. F. Pierret, *Semiconductor Device Fundamentals* (Addison-Wesley, Reading, MA, 1996).
[17]Y. Izawa, Y. Setuhara, M. Hashida, M. Fujita, and Y. Izawa, Jpn. J. Appl. Phys. Part 1 **45**, 5791 (2006).
[18]J. Bonse, K.-W. Brzezinka, and A. J. Meixner, Appl. Surf. Sci. **221**, 215 (2004).
[19]J. Bonse, S. Baudach, J. Krüger, W. Kautek, and M. Lenzner, Appl. Phys. A **74**, 19 (2002).
[20]B. Adams, S. Wright, and K. Kunze, Metall. Mater. Trans. A **24**, 819 (1993).
[21]S. I. Wright and M. M. Nowell, Microsc. Microanal. **12**, 72 (2006).
[22]M. T. Winkler, M.-J. Sher, Y.-T. Lin, M. J. Smith, H. Zhang, S. Gradečak, and E. Mazur, J. Appl. Phys. **111**, 93511 (2012).
[23]Y. Izawa, Y. Izawa, Y. Setsuhara, M. Hashida, M. Fujita, R. Sasaki, H. Nagai, and M. Yoshida, Appl. Phys. Lett. **90**, 044107 (2007).
[24]U. Köster, Phys. Status Solidi A **48**, 313 (1978).
[25]A. V. Zotov and V. V. Korobtsov, J. Cryst. Growth **98**, 519 (1989).